ELSEVIER

Journal of Alloys and Compounds 262–263 (1997) 219–224

Journal of ALLOYS AND COMPOUNDS

Neutron powder diffraction study of the antiferromagnetic compound $Tb_2Pd_{2.05}Sn_{0.95}$

D. Laffargue[a,b], T. Roisnel[a,*], B. Chevalier[b], F. Bourée[a]

[a] *Laboratoire Léon Brillouin (CEA / CNRS), CEA-Saclay, 91191 Gif-sur-Yvette Cedex, France*

[b] *Institut de Chimie de la Matière Condensée de Bordeaux, CNRS [UPR 9048], Université de Bordeaux I, Avenue du Dr. Schweitzer, 33608 Pessac, France*

Abstract

Magnetic measurements and neutron diffraction experiments have been performed on a $Tb_2Pd_{2.05}Sn_{0.95}$ polycrystalline sample. Two antiferromagnetic transitions are obtained at $T_N = 27.3(2)$ K and $T_2 = 20.8(5)$ K, respectively. The magnetic structure between T_N and T_2 is characterized by an incommensurate wave vector $\mathbf{k}_1 = (k_x\ k_x\ 1/2)$ (with a continuous decrease of the incommensurate component k_x from $k_x = 0.115(5)$ at $T = 26.3$ K to $k_x = 0.070(5)$ at $T = 20.8$ K). Below T_2, a commensurate magnetic structure is observed, with $\mathbf{k}_2 = (0\ 0\ 1/2)$ wave vector (k_x locked to zero). This low temperature magnetic structure is described as a non-collinear arrangement of terbium magnetic moments along the [110] and [1$\bar{1}$0] directions of the tetragonal unit cell, according to the Γ_{10} irreducible representation of the wave vector group. The value of the ordered magnetic moment is equal to 8.70(5) μ_B/Tb^{3+} at $T = 1.5$ K. © 1997 Elsevier Science S.A.

Keywords: Neutron powder diffraction; Magnetic structure; Antiferromagnetism; Intermetallic compound

1. Introduction

U_2M_2X intermetallic compounds (M = 3d or 4d transition element and X = Sn, In), which crystallize in a tetragonal ordered structure derived from U_3Si_2-type structure (P4/mbm space group), have been extensively studied over the last few years, by electrical resistivity, specific heat and magnetic measurements as well as by X-ray and neutron diffraction [1–6].

Magnetically ordered U_2M_2Sn compounds are antiferromagnetic, with magnetic structures depending on the nature of the transition element M. The magnetic structures of U_2Ni_2Sn and U_2Rh_2Sn are described as a collinear arrangement of uranium magnetic moments with $\mathbf{k} = (0\ 0\ 1/2)$ wave vector [5,6,8], while a $\mathbf{k} = (0\ 0\ 0)$ non-collinear magnetic structure is observed for U_2Pd_2Sn [7].

The Rare-Earth (RE) based stannides $RE_2Pd_{2+x}Sn_{1-x}$ exist with RE = Ce, Nd, Gd, Tb, Dy, Ho and Er. All these compounds are isostructural and adopt for $x \neq 0$ a new superstructure of U_3Si_2 type [9], thus allowing a comparative study of the influence of RE nature on the magnetic properties in the series. $Ce_2Pd_{2+x}Sn_{1-x}$ compounds, for instance, have been prepared within a large range of homogeneity on the palladium-rich side [$0.04(3) \leq x \leq 0.21(4)$], with magnetic properties dependant on the chemical composition [10]. The magnetic structures of the series $RE_2Pd_{2+x}Sn_{1-x}$ have been published only for the compound $Ce_2Pd_{2.04}Sn_{0.96}$ [11], for which the cerium magnetic moments are parallel to the tetragonal axis and arranged either in an incommensurate $\mathbf{k} = (k_x\ 0\ 0)$ antiferromagnetic structure between $T_N = 4.8(2)$ K and $T_C = 3.0(2)$ K, or a ferromagnetic structure below T_C.

Here we show magnetic measurements and neutron diffraction experiments performed on a $Tb_2Pd_{2.05}Sn_{0.95}$ polycrystalline sample.

* Corresponding author.

PII S0925-8388(97)00385-X

2. Experimental part

The sample was prepared by arc-melting stoechiometric amounts of the constituent elements under a argon atmosphere. The obtained alloy was then annealed for 4 weeks at 800°C in a quartz crucible sealed under vacuum.

Magnetization measurements were carried out in the 2–35 K temperature range using a Superconducting Quantum Interference Device (SQUID) magnetometer.

Neutron diffraction experiments have been performed at the Orphée reactor (Saclay, France), on the 3T2 (High Resolution Powder Diffractometer, $\lambda = 1.2272$ Å) and G41 (800 cells PSD, $\lambda = 2.425$ Å) two-axis diffractometers [12]. Neutron data were analyzed with the Rietveld-type FULLPROF program [13], using the neutron scattering lengths from [14]: $b_{Tb} = 0.738\ 10^{-12}$ cm, $b_{Pd} = 0.591\ 10^{-12}$ cm and $b_{Sn} = 0.6225\ 10^{-12}$ cm. The magnetic form factor for Tb^{3+} was calculated in the dipolar approximation with the $\langle j_0 \rangle$ and $\langle j_2 \rangle$ values extracted from [15].

3. Crystal structure

The $Tb_2Pd_{2.05}Sn_{0.95}$ neutron powder diffraction pattern at room temperature is shown in Fig. 1. FULLPROF analysis of these data, on the basis of U_3Si_2 derived structure (P4/mbm space group) of [10], leads to the structural parameters (cell parameters, atomic positions, isotropic thermal factors and occupation numbers) listed in Table 1.

4. Magnetic measurements

The thermal dependence of the magnetic susceptibility, obtained with an external applied field of 250 G, is represented in Fig. 2. It shows a pronounced maximum at $T_N = 27.5(5)$ K, characteristic of antiferromagnetic ordering. At lower temperatures, a small kink in the $\chi = f(T)$ curve is observed at $T_2 = 23.5(5)$ K, which can be attributed to another magnetic transition in the sample.

From higher temperature magnetic susceptibility data, an effective experimental magnetic moment ($\mu_{eff.exp.} = 10.15\ \mu_B$/terbium) is deduced, in good agreement with the Tb^{3+} free ion theoretical value ($\mu_{eff.th.} = 9.72\ \mu_B$). As expected, the paramagnetic Curie temperature is found to be negative ($\theta_p = -13$ K).

5. Magnetic structures

Medium resolution neutron powder diffraction patterns ($\lambda = 2.425$ Å) for $Tb_2Pd_{2.05}Sn_{0.95}$ have been recorded in the 1.5–31 K low temperature range. These patterns (Fig. 3) clearly show the existence of new Bragg peaks, connected to 3D antiferromagnetic ordering in $Tb_2Pd_{2.05}Sn_{0.95}$. This antiferromagnetic order is temperature-dependent, as seen in Fig. 3. All the magnetic Bragg peaks below $T_N = 27.3(2)$ K can be effectively indexed with the help of a $\mathbf{k} = (k, k, 1/2)$-type wavevector; k values are incommensurate in the higher temperature range ($20.8(5)\ \text{K} \leq T \leq T_N$) and commensurate at lower

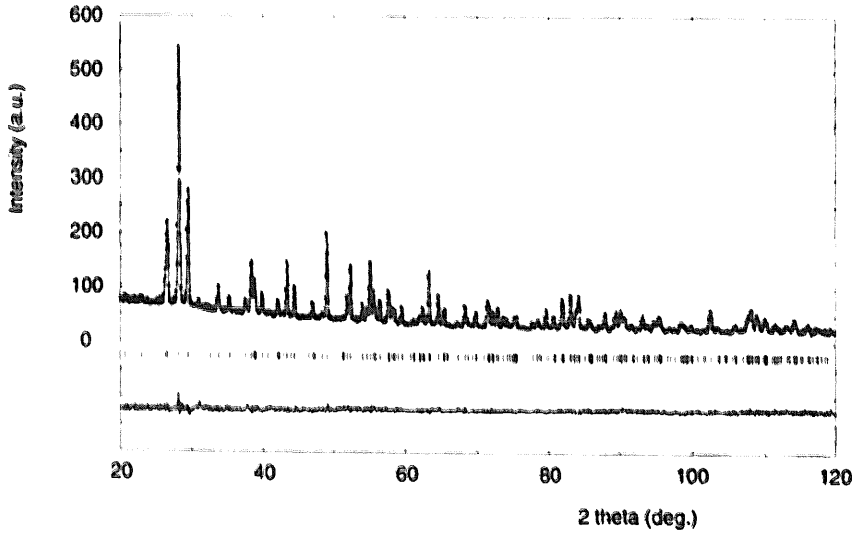

Fig. 1. $Tb_2Pd_{2.05}Sn_{0.95}$ neutron powder diffraction pattern ($\lambda = 1.2272$ Å) at room temperature (experimental points, calculated and difference profiles; vertical ticks for $2\theta_B$ Bragg positions in the P4/mbm space group).

Table 1
$Tb_2Pd_{2.05}Sn_{0.95}$ structural parameters at room temperature (from 3T2 high resolution neutron powder diffraction data)

P4/mbm space group [a = 7.6333(3) Å; c = 3.7374(2) Å]						
Atom	Site	x	y	z	Biso (Å^2)	Occupation (%)
Tb	(4h)	0.1747(2)	0.6747(2)	0.5	0.73(4)	1
Pd1	(4g)	0.3726(3)	0.8726(3)	0	0.99(6)	1
Sn	(2a)	0	0	0	0.99(6)	0.972(7)
Pd2	(4e)	0	0	0.26(6)	0.99(6)	0.014(7)

$R_N = 5.1\%$; $\chi^2 = 1.34$.

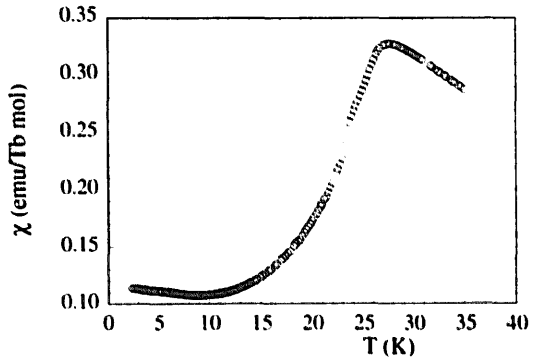

Fig. 2. Thermal variation of the magnetic susceptibility of $Tb_2Pd_{2.05}Sn_{0.95}$ (external field H = 250 G).

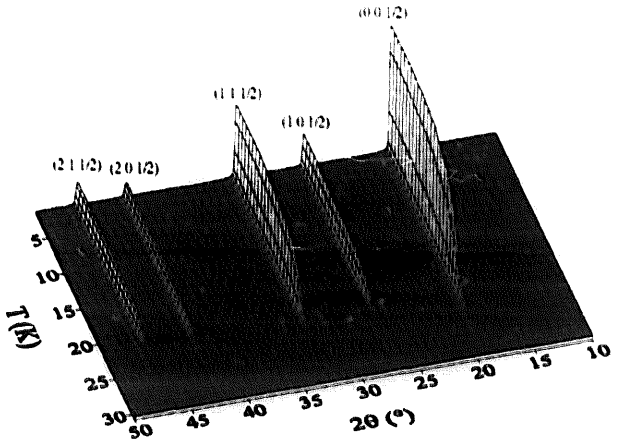

Fig. 3. $Tb_2Pd_{2.05}Sn_{0.95}$ neutron powder diffraction patterns (λ = 2.425 Å) vs. temperature: incommensurate ($20.8(5) < T(K) < T_N = 27.3(2)$) and commensurate ($T < T_2 = 20.8(5)$ K) magnetic phases are clearly seen in the figure.

temperatures [$T \leq 23.6(5)$ K]. A region of coexistence of incommensurate $\mathbf{k}_1 = (k_x\ k_x\ 1/2)$ and commensurate $\mathbf{k}_2 = (0\ 0\ 1/2)$ wave vectors is then observed, which could be due to chemical inhomogeneities in the sample.

Thermal variations of the d_{hkl}-spacing and integrated intensity of the most intense magnetic Bragg peak $(0\ 0\ 0)^-$, are plotted in Fig. 4a and Fig. 4b. A large increase of $d_{(0\ 0\ 0)^-}$ is observed below T_N down to $T_2 = 20.8(5)$ K, as a consequence of a continuous decrease of the incommensurate k_x component in this temperature range (from $k_x = 0.115(5)$ at $T = 26.3$ K to $k_x = 0.070(5)$ at $T = 20.8$ K). Below T_2, $d_{(0\ 0\ 0)^-}$ is independent of temperature, corresponding to $d_{(0\ 0\ 1/2)}$ only, i.e. to the commensurate $\mathbf{k}_2 = (0\ 0\ 1/2)$ antiferromagnetic structure of $Tb_2Pd_{2.05}Sn_{0.95}$.

The coexistence of the two wavevectors $\mathbf{k}_1 = (k_x\ k_x\ 1/2)$, with $k_x \neq 0$ and $\mathbf{k}_2 = (0\ 0\ 1/2)$ is evidenced by the plot in Fig. 5 [$T = 22.1$ K; $k_x = 0.072(5)$].

Possible magnetic arrangements for the wave vector $\mathbf{k} = (0\ 0\ 1/2)$ and magnetic moments located in (*4h*) Wyckoff position (P4/mbm space group), have been previously described by Bourée et al. [5], using representation group theory arguments. All of these magnetic structures correspond to magnetic moments directed either parallel (Γ_2, Γ_8, Γ_9), or perpendicular (Γ_1, Γ_3, Γ_5, Γ_7, Γ_{10}) to the tetragonal c-axis.

The existence of the (0 0 1/2) magnetic Bragg peaks in the neutron diffraction patterns of $Tb_2Pd_{2.05}Sn_{0.95}$ clearly shows that Tb^{3+} magnetic moments are not parallel to the c-axis; and leads to exclude any irreducible representation with:

$$\sum_{i=1}^{4} \mathbf{M}_i = 0,$$

where $\mathbf{M}_i$ stands for the magnetic moments located at ($i = 1$: Tb_1) [x $1/2+x$ $1/2$], ($i = 2$: Tb_2) [$-x$ $1/2-x$ $1/2$], ($i = 3$: Tb_3) [$1/2+x$ $-x$ $1/2$] and ($i = 4$: Tb_4) [$1/2-x$ x $1/2$] Tb^{3+} atomic positions. The only possibility is then Γ_{10}, which gives magnetic moments $\mathbf{M}_1 = \mathbf{M}_2$ and $\mathbf{M}_3 = \mathbf{M}_4$. The best fit between observed and calculated data is obtained with the non-collinear arrangement of the magnetic moments given below:

	m_x	m_y	m_z
$\mathbf{M}_1$:	m	m	0
$\mathbf{M}_2$:	m	m	0
$\mathbf{M}_3$:	m	$-m$	0
$\mathbf{M}_4$:	m	$-m$	0

Terbium magnetic moments are then aligned along [110] or [1$\bar{1}$0] directions (Fig. 6). This 'Γ_{10}' magnetic model is independent of temperature below T_2, except for the value of m. Refinement of neutron data

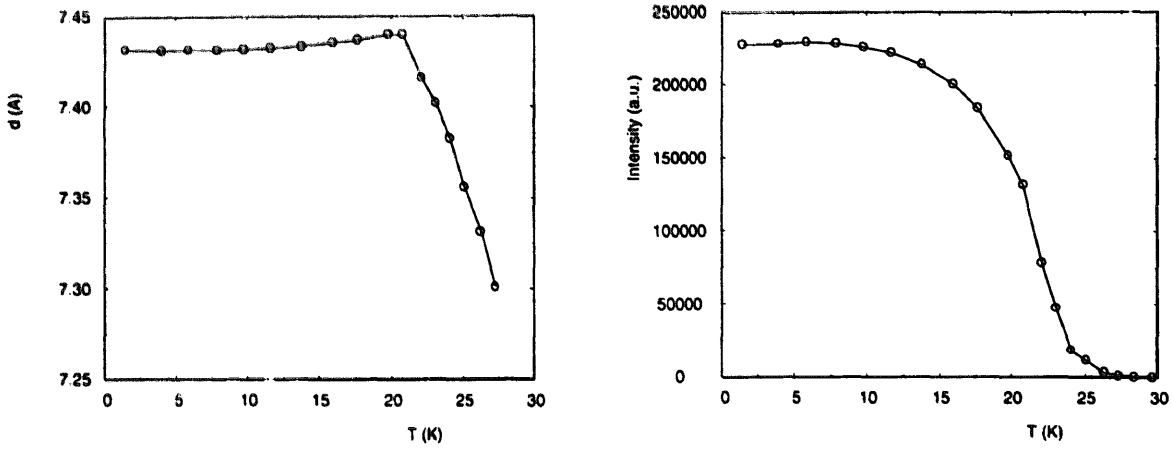

Fig. 4. a: Thermal variation of the $d_{(0\,0\,0)^{\pm}}$ spacing; b: thermal variation of $(0\,0\,0)^{\pm}$ magnetic Bragg peak integrated intensity.

at $T = 1.5$ K (Fig. 7) leads to $M = m\sqrt{2} = 8.70(5)\ \mu_B$, in good agreement with the Tb^{3+} free ion saturated moment value ($g_J J = 9\ \mu_B$).

6. Conclusion

Two antiferromagnetic transitions have been observed for polycrystalline $Tb_2Pd_{2.05}Sn_{0.95}$ by means of magnetic measurements and neutron diffraction experiments. The $Tb_2Pd_{2.05}Sn_{0.95}$ low temperature magnetic phase ($T < T_2 = 20.8(5)$ K) is associated with $\mathbf{k}_2 = (0\ 0\ 1/2)$ commensurate wave vector, Γ_{10} irreducible representation (magnetic group theory). Magnetic moments for Tb^{3+} ions are perpendicular to the tetragonal c-axis, and directed along [110] ($M_1 = M_2$) or [1$\bar{1}$0] ($M_3 = M_4$), with $M = 8.70(5)\ \mu_B/Tb^{3+}$ at $T = 1.5$ K. Between T_2 and $T_N = 27.3(2)$ K, an incommensurate magnetic structure is observed, with $\mathbf{k}_1 = (k_x\ k_x\ 1/2)$, and k_x decreasing with decreasing temperatures.

The same sequence of magnetic structures, with incommensurate magnetic wave vector at higher temperatures ($T_C \le T \le T_N$) and lock-in effect at low temperatures (from $k_x \neq 0$ to $k_x = 0$ below T_C), was previously observed for $Ce_2Pd_{2.04}Sn_{0.96}$, with (k_x 0 0)-type magnetic wave vector in that case and Ce^{3+} magnetic moments parallel to the c-axis.

The existence of incommensurate magnetic structures in 2:2:1 stannides, U_2M_2Sn and RE_2M_2Sn, occurs only for Rare Earth (RE) compounds. Only two commensurate magnetic wave vectors are necessary to describe the U_2M_2Sn (M = Ni, Rh, Pd) antiferromagnetic structures: $\mathbf{k} = (0\ 0\ 0)$ and $\mathbf{k} = (0\ 0\ 1/2)$. It should be noted that $Tb_2Pd_{2.05}Sn_{0.95}$

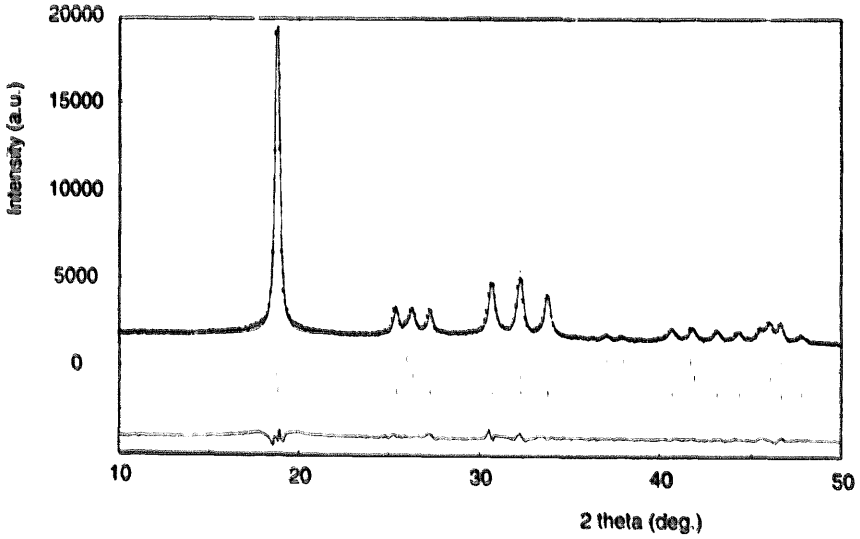

Fig. 5. Refinement (in profile matching mode [13]) of $Tb_2Pd_{2.05}Sn_{0.95}$ neutron powder diffraction pattern at $T = 22.1$ K. Vertical ticks (from up to down) correspond to $2\theta_B$ Bragg positions for P4/mbm crystal structure, $\mathbf{k}_2 = (0\ 0\ 1/2)$ commensurate and $\mathbf{k}_1 = (k_x\ k_x\ 1/2)$ incommensurate magnetic phases.

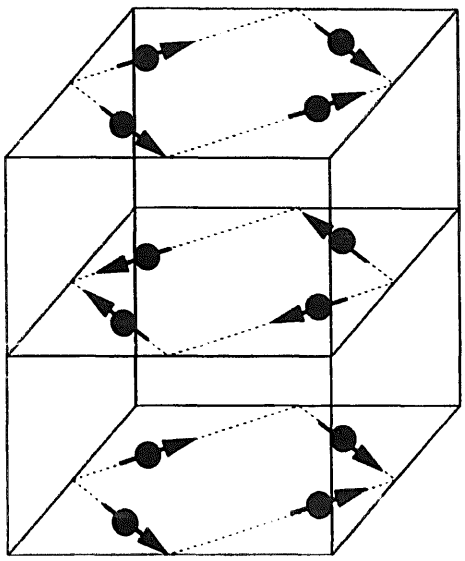

Fig. 6. Schematic representation of the commensurate [k = (0 0 1/2)] non-collinear magnetic structure of $Tb_2Pd_{2.05}Sn_{0.95}$ (magnetic unit-cell a × a × 2c).

is antiferromagnetic, but with a 'new' k = (0 0 1/2) magnetic structure, as compared to U_2Ni_2Sn and U_2Rh_2Sn k = (0 0 1/2) magnetic structures (Γ_8).

If the U_2M_2Sn physical properties are strongly dependent on the nature of M via 5f(U)–nd(M) hybridization, hybridization effects are no longer relevant for RE_2M_2Sn compounds, mainly with RE in the second series. Models for localized 4f magnetism, with competing magnetic interaction and Crystalline Electric Field (CEF) anisotropy, have then to be considered. The incommensurate modulation observed for $Tb_2Pd_{2.05}Sn_{0.95}$ suggests a RKKY model for magnetic exchange (via conduction electrons). As regards CEF for P4/nbm space group, the point symmetry of (*4h*) Wickoff position is *mm*, with one mirror perpendicular to the tetragonal c-axis and the other either perpendicular to [1$\bar{1}$0] (for Tb_1 and Tb_2) or [110] directions (for Tb_3 and Tb_4). Easy magnetization axis could then be [110] for Tb_1 and Tb_2 magnetic moments and [1$\bar{1}$0] for Tb_3 and Tb_4 magnetic moments: these directions are the directions effectively observed for the magnetic moments in $Tb_2Pd_{2.05}Sn_{0.95}$. The value of the Tb^{3+} magnetic moment (8.70 μ_B/Tb^{3+} at $T = 1.5$ K), close to the free ion theoretical value (9 μ_B/Tb^{3+}), indicates, however, a rather small overall CEF splitting, as compared to magnetic exchange in this compound ($\sim k_B T_N$).

References

[1] F. Mirambet, B. Chevalier, L. Fournès, P. Gravereau, J. Etourneau, J. Alloys Comp. 203 (1994) 29–33.

[2] F. Mirambet, L. Fournès, B. Chevalier, P. Gravereau, J. Etourneau, J. Magn. Magn. Mater. 138 (1994) 244–254.

[3] R.P. Pinto, M.M. Amado, M.A. Salguiero, M.E. Braga, J.B. Sousa, B. Chevalier, F. Mirambet, J. Etourneau, J. Magn. Magn. Mater. 140/144 (1994) 1371–1372.

[4] H. Nakotte, K. Prokes, E. Bruck, N. Tang, F.R. de Boer, P. Svoboda, V. Sechovsky, L. Havela, J.M. Winand, A. Seret, J. Rebizant, J.C. Spirlet, Physica B 201 (1994) 247–250.

[5] F. Bourée, B. Chevalier, L. Fournès, F. Mirambet, T. Roisnel, V.H. Tran, Z. Zolnierek, J. Magn. Magn. Mater. 138 (1994) 307.

[6] H. Nakotte, A. Purwanto, R.A. Robinson, K. Prokes, J.C.P. Klaasse, P.F. de Chatel, F.R. de Boer, L. Havela, V. Sechovsky, L.C.J. Pereira, A. Seret, J. Rebizant, J.S. Spirlet, F. Trouw, Phys. Rev. B 53 (1996) 3263–3271.

[7] A. Purwanto, R.A. Robinson, L. Havela, V. Sechovsky, P. Svoboda, H. Nakotte, K. Prokes, F.R. de Boer, A. Seret, J.M.

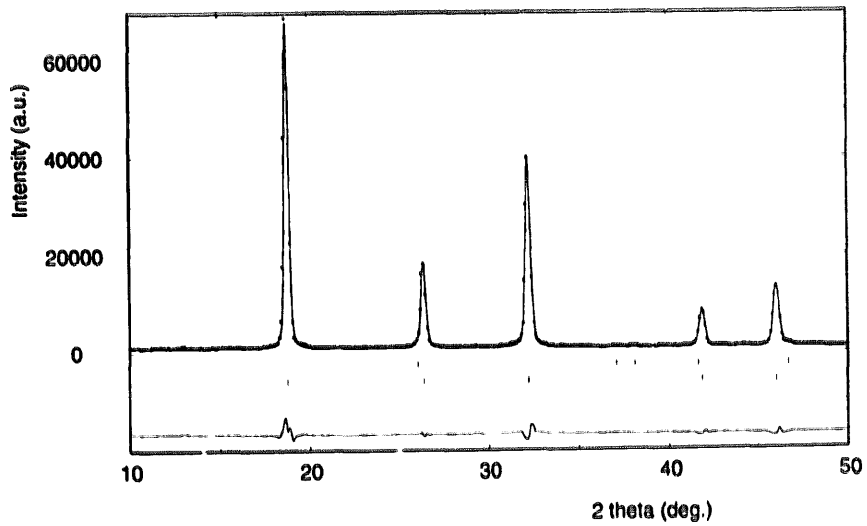

Fig. 7. $Tb_2Pd_{2.05}Sn_{0.95}$ neutron powder diffraction pattern ($\lambda = 2.425$ Å; $T = 1.5$ K): experimental points; calculated and difference profiles; vertical ticks for $2\theta_B$ Bragg positions, for both crystal (P4/nbm space group; ticks above) and magnetic structures (commensurate k = (0 0 1/2) canted magnetic structure of Fig. 6; ticks below). ($R_N = 3.1\%$ and $R_M = 3.2\%$, calculated from the whole diffraction pattern data [10–90° 2θ range]).

Winand, J. Rebizant, J.C. Spirlet, Phys. Rev. B 50 (1994) 6792–6801.
[8] L.C.J. Pereira, J.A. Paixao, P. Estrela, M. Godhinho, F. Bourdarot, M. Bonnet, J. Rebizant, J.C. Spirlet, M. Almeida, J. Phys. Cond. Matter 8 (1996) 11167–11179.
[9] F. Fourgeot, Thèse n°1576, Université de Bordeaux I, France, 1996.
[10] F. Fourgeot, P. Gravereau, B. Chevalier, L. Fournès, J. Etourneau, J. Alloys Comp. 238 (1996) 102–109.
[11] D. Laffargue, F. Fourgeot, F. Bourée, B. Chevalier, T. Roisnel, J. Etourneau, Solid State Comm. 100 (1996) 575–579.
[12] T. Roisnel, J. Rodriguez-Carvajal, M. Pinot, G. André, F. Bourée, Mat. Sci. Forum. 166/169 (1994) 245–250.
[13] J. Rodriguez-Carvajal, Physica B 192 (1993) 55–69.
[14] V.F. Sears, Neutron News 3 (1992) 26.
[15] A.J. Freeman, J.P. Desclaux, J. Magn. Magn. Mater. 12 (1979) 11.